Regenerative Therapy 26 (2024) 520–532

Contents lists available at ScienceDirect

Regenerative Therapy

journal homepage: http://www.elsevier.com/locate/reth

Original Article

Topical application of a hyaluronic acid-based hydrogel integrated with secretome of human mesenchymal stromal cells for diabetic ulcer repair

Fabio Salvatore Palumbo [a], Matteo Calligaris [b], Laura Calzà [c, d], Calogero Fiorica [a], Vito Antonio Baldassarro [e], Anna Paola Carreca [f], Luca Lorenzini [e], Alessandro Giuliani [e], Claudia Carcione [g], Nicola Cuscino [h], Giovanna Pitarresi [a], Simone Dario Scilabra [b], Pier Giulio Conaldi [h], Cinzia Maria Chinnici [g, *]

[a] Dipartimento di Scienze e Tecnologie Biologiche Chimiche e Farmaceutiche (STEBICEF), Università degli Studi di Palermo, via Archirafi 32, 90123, Palermo, Italy
[b] Proteomic Group, Ri.MED Foundation c/o IRCCS ISMETT, via E. Tricomi 5, 90127, Palermo, Italy
[c] Fondazione IRET, Tecnopolo di Bologna, Via Tolara di Sopra, 41e, 40064, Ozzano dell'Emilia (BO), Italy
[d] Dipartimento di Farmacia e Biotecnologie (FABIT), Università degli Studi di Bologna, Via S. Donato, 15, 40127, Bologna, Italy
[e] Dipartimento di Scienze Mediche Veterinarie (DIMEVET), Università degli Studi di Bologna, Bologna, Italy
[f] Regenerative Medicine and Immmunotherapy Unit, Ri.MED Foundation c/o IRCCS ISMETT, via E. Tricomi 5, 90127, Palermo, Italy
[g] Cell Therapy Group, Ri.MED Foundation c/o IRCCS ISMETT, via E. Tricomi, 5 90127, Palermo, Italy
[h] Department of Research, IRCCS ISMETT, Via E. Tricomi 5, 90127, Palermo, Italy

ARTICLE INFO

Article history:
Received 8 April 2024
Received in revised form
2 July 2024
Accepted 18 July 2024

Keywords:
Hyaluronic acid hydrogel
Mesenchymal stromal cell secretome
Wound healing
Diabetic mice
Skin ulcer
Proteomics

ABSTRACT

This preclinical proof-of-concept study aimed to evaluate the effectiveness of secretome therapy in diabetic mice with pressure ulcers. We utilized a custom-made hyaluronic acid (HA)-based porous sponge, which was rehydrated either with normal culture medium or secretome derived from human mesenchymal stromal cells (MSCs) to achieve a hydrogel consistency. Following application onto skin ulcers, both the hydrogel-only and the hydrogel + secretome combination accelerated wound closure compared to the vehicle group. Notably, the presence of secretome significantly enhanced the healing effect of the hydrogel, as evidenced by a thicker epidermis and increased revascularization of the healed area compared to the vehicle group. Notably, molecular analysis of healed skin revealed significant downregulation of genes involved in delayed wound healing and abnormal inflammatory response in ulcers treated with the hydrogel + secretome combination, compared to those treated with the hydrogel only. Additionally, we found no significant differences in therapeutic outcomes when comparing the use of secretome from fetal dermal MSCs to that from umbilical cord MSCs. This observation is supported by the proteomic profile of the two secretomes, which suggests a shared molecular signature responsible of the observed therapeutic effects.

1. Introduction

Chronic skin wounds, often associated with systemic conditions such as diabetes and vasculitis, or complications of surgical procedures and aging [1], pose a significant clinical challenge. With the aging of global population and the increasing prevalence of diabetes, the incidence of chronic skin wounds is expected to rise soon [2]. Despite various experimental treatments, only three have received approval from the Food and Drugs Administration (FDA): two skin substitutes, Apligraf and Dermagraft, and one based on recombinant human platelet-derived growth factor (PDGF) known as REGRANEX [3]. Nevertheless, approximately 50% of chronic skin wounds remain unresponsive to these treatments [4], highlighting the urgent need for innovative therapeutic approaches covering this clinic area. The primary goal of wound healing is to achieve

* Corresponding author. Cell Therapy Group, Ri.MED Foundation, Via E. Tricomi, 5, 90127, Palermo, Italy.
E-mail address: cchinnici@fondazionerimed.com (C.M. Chinnici).
Peer review under responsibility of the Japanese Society for Regenerative Medicine.

https://doi.org/10.1016/j.reth.2024.07.008

rapid wound closure, minimizing the risks of further damage or infection, which could otherwise delay the healing process. Additionally, the newly repaired tissue should ideally exhibit both functional capabilities and a visual appearance closely resembling that of healthy skin [5]. Delayed wound healing can result from various factors, including impaired angiogenesis, altered the local cytokine milieu, reduced fibroblasts migration and altered extracellular matrix (ECM) deposition. Disruption in any wound healing phase can lead to delayed wound healing, ultimately leading to the development of chronic wounds [6]. Initially thought as distinct steps, recent insights have suggested that the four phases of wound healing (homeostasis, inflammation, proliferation and remodeling) largely overlap and influence each other. Consequently, therapeutic approaches that simultaneously target all four phases hold promise for promoting wound healing.

Mesenchymal stromal cell (MSC) secretome holds therapeutic potential across a range of clinical applications [7,8] The MSC secretome is recognized as a novel booster for regenerative medicine [9], harnessing the body's innate regenerative capacity. As a cell-free approach, secretome-based therapy offers distinct advantages over conventional cell therapy, particularly in terms of safety, as it can avoid the need for cell transplantation. The clinical development of secretome-based therapy for skin wound healing is in its early stages, with its evaluation limited to two registered clinical trials of safety and efficacy [10,11]. In this study, we assessed feasibility and efficacy of secretome therapy in a diabetic foot ulcer model, using genetically diabetic mice (C57BL/KsJ-m+/+Leprdb, db/db) with pressure ulcers [12–14]. This model, widely used in experimental ulcers research, is characterized by impaired expression of hypoxia-related and ECM genes, reduced vascularization, and a prolonged inflammatory phase delaying the progression toward subsequent wound healing phases [2,14]. Furthermore, to ensure secretome delivery, we utilized a custom-made hydrogel of hyaluronic acid (HA) [15,16]. HA, a predominant ECM constituent, plays a crucial role in tissue repair by regulating cell apoptosis, proliferation, migration, and vascularization [17,18]. This remarkable potential led to the development of a spectrum of clinically relevant HA-based biomaterials, particularly in the context of cosmetic applications for skincare and wound healing [19–24]. However, while the effects of HA on skin wound healing are largely documented, there are only two animal studies demonstrating the healing effect of HA hydrogels combined with MSC secretome on diabetic wounds [25,26].

Batches of freeze-dried HA sponges and secretome from fetal dermal (FD) and umbilical cord (UC)-MSCs were prepared in advance as read-to-use formulations. Following integration with the appropriate volume of secretome, the resulting hydrogels were directly applied to the ulcer site. Healing parameters, including re-epithelialization time, epidermal thickness, the presence of dermal annexes, and angiogenesis, were evaluated through visual inspection, histology, and immunofluorescence analysis in ulcers treated with a vehicle, hydrogel-only or the hydrogel + secretome combination. Finally, to gain insights into molecular signatures associated with secretome-based therapy, proteomic profiling of the two MSC secretome types, as well as gene expression analysis of the healed ulcers were conducted.

2. Methods

2.1. Production of HA-based hydrogel patches for secretome delivery

A porous sponge-like material made of HA was synthesized by freeze-drying as previously described [27] (supplementary material S1). Integration of the sponge with secretome resulted in the immediate formation of a hydrogel, sustaining secretome release (Fig. 1A and B). Release kinetics of secretome is detailed elsewhere [28]. Batches of freeze-dried sponges were stored at −80 °C and shipped frozen for *in vivo* experiments.

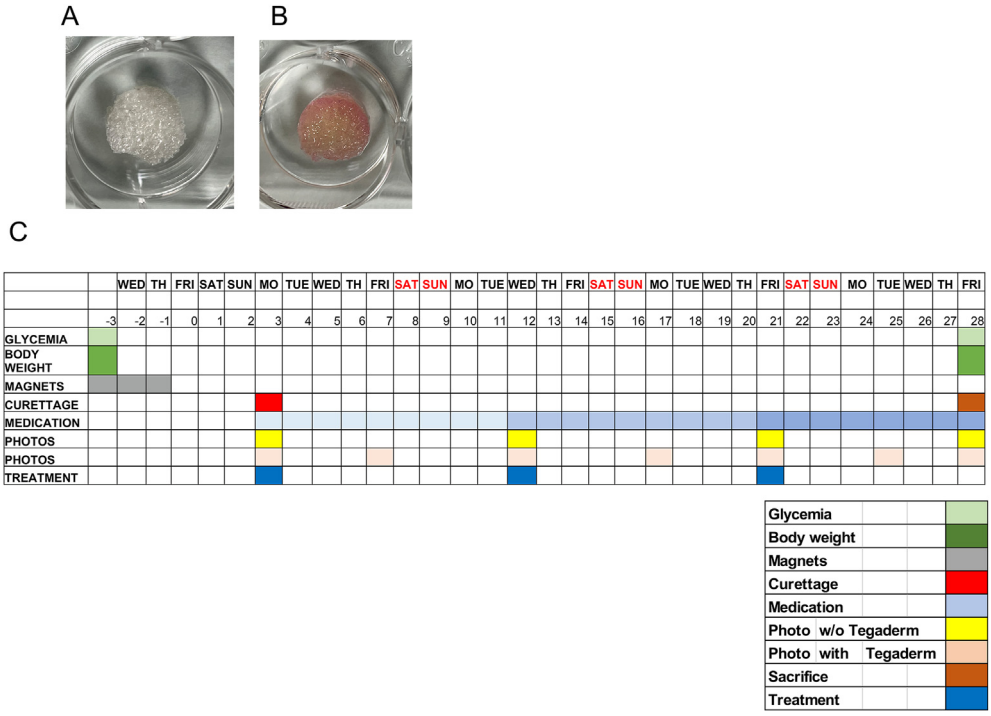

Fig. 1. (A) HA freeze-dried sponge. (B) Secretome-rehydrated sponge acquiring hydrogel consistency. (C) Eperimental timeline, including the treatments administered during the study along with its corresponding timing.

2.2. Secretome collection and Luminex-based characterization

Human MSCs were isolated from fetal dermis and umbilical cord following a protocol approved by IRCCS ISMETT's Institutional Review Research Board, as previously described [29,30]. Secretome was collected as previously described [30]. Briefly, serum-free alpha-Minimum Essential Medium (MEM) (Gibco, Thermo Fisher Scientific, Waltham, MA, USA) was added to 80% confluent cells into 175 cm^2 sterile tissue culture flasks (Costar Corning Inc., Costar, NY, USA), collected 24 h later, and centrifuged to remove debris. Quantification of secretome was performed using a Luminex immunoassay (Luminex 200; Luminex Corp. Austin, TX, USA), while its biological activity was assessed through xCELLigence real-time cell migration, as previously described [30]. Secretome from six independent FD-MSC and UC-MSC donors, which exhibited significant amounts of bioactive factors (Table 1) and a consistent biological activity (cell index of approximately 2.0; data not shown) was pooled and concentrated 10-fold using Amicon Ultra-15 Centrifugal filters with a 3 kDa cut-off (Millipore, Billerica, MA, USA). Batches of secretome were stored at −80 °C and shipped frozen for the *in vivo* experiments.

2.3. Proteomic profiling of secretome

Secretomes from both cell types were processed by filter-aided sample preparation (FASP) [31] and STAGE-tips (Accession Number: 12585499), and then analyzed by liquid chromatography tandem mass spectrometry (LC-MS/MS) and label-free quantification (LFQ), as previously described [32,33]. Briefly, 2 ml of secretome were applied to Vivacon spin columns with a 10 kDa filter cut-off (Sartorius, Gottinga, Germany). After concentration, the proteins were reduced and alkylated before a sequential digestion with 0.2 μg LysC and 0.1 μg trypsin (Promega, Madison, Wisconsin, USA). Tryptic peptides were collected from filter columns after centrifugation, acidified and applied for desalting to stop-and-go extraction (STAGE) tips packed in-house with Empore C18 disks (Merck, Sigma–Aldrich, St Louis, Missouri, USA), as previously described [34]. After elution, tryptic peptides were quantified with a Nanodrop 2000 (Thermo Fisher Scientific) and 1.5 μg peptides were loaded onto a Dionex Ultimate 3000 RSLC nano LC system coupled online to a Q-Exactive + mass spectrometer (Thermo Fisher Scientific). Peptides were separated on Acclaim PEPMap C18 column (50 cm × 75 μm ID, Thermo Scientific) with 250 nL/min flow using a binary gradient of water (A) and acetonitrile (B) supplemented with 0.1% formic acid for 350 min. Data-dependent acquisition (DDA) was used for LFQ. Raw data were analyzed with Maxquant software, version 2.0.1.0 (maxquant.org, Max-Planck Institute Munich) [35], and searched against a reviewed canonical fasta database of *Homo sapiens* from UniProt (download: 5th November 2020). Proteins differentially abundant in secretome of UC-MSCs versus FD-MSCs were analyzed for their association with Kyoto Encyclopedia of Genes and Genomes (KEGG) and Gene Ontology (GO) pathways and biological processes (GOBP) using the Enrichr webserver [36] and plotted according to their q-value and Odds ratio. To analyze differences between the secretomes of UC-MSCs and FD-MSCs LFQ intensities were log_2 transformed and plotted against the -Log_{10} p-value of their change. A false discovery rate (FDR)-adjusted p-value of 0.05 was set as the threshold for statistical significance.

2.4. Animals, lesions and monitoring

Animal protocols adhered to the European Community Council Directives (2010/63/EU), followed the ARRIVE guidelines, and complied with the NIH Guide for the Care and Use of Laboratory Animals, and approved by the Italian Ministry of Health (authorization no. 155/2021-PR). We used 11-week-old genetically diabetic C57BL/KsJ-m+/+Leprdb (db/db) male mice (Calco-Lecco; Charles River Laboratories). The animals were housed with access to food pellets and water *ad libitum* and maintained on a 12-h dark–light cycle, as previously described [14]. Blood glucose levels were measured prior to treatments using Contour XT (Bayer, Basel, Switzerland). For lesion induction, mice were deeply anesthetized (isoflurane 3% *plus* 2 l/min O_2), shaved on the back, and the area was thoroughly cleansed. Pressure ulcers were induced using two magnetic disks, each of a diameter of 12 mm (anisotropic ferrite) and a thickness of 5.0 mm, with an average weight of 2.4 g and 1000 G magnetic force (Algamagnetic, Italy), as previously described [14]. A skin fold was gently raised and placed between the two magnets, ensuring a 1.0 cm skin bridge between the magnets to generate a compressive pressure of 50 mm Hg between the two plates, which is necessary to cause local tissue ischemia [2]. Three ischemia-reperfusion (I/R) cycles were used, with each single I/R cycle consisting of a 12-h period of magnet placement followed by a 12-h rest period. On day 3 following the final I/R cycle, a surgical wound curettage was performed to remove the ischemic skin and eschar.

2.5. Experimental groups and treatments

The study included the following experimental groups, each consisting of 8 animals, and each mouse had two dorsal ulcers (n = 16 ulcers) in accordance with the power analysis for sample size calculation:

- control, intact animals
- db/db mice + vehicle
- db/db mice + hydrogel
- db/db mice + hydrogel + FD-MSC secretome
- db/db mice + hydrogel + UC-MSC secretome

Mice were randomly assigned to the experimental groups after lesion induction. The topical application of the hydrogel began on day 3 after the last I/R cycle and was repeated every 9 days for a

Table 1
Luminex-based quantification of secretomes of UC-MSCs and FD-MSCs with a focus on VEGF-A and SDF-1 alpha.

UC-MSC SEC	**#1**	**#2**	**#3**	**#4**	**#5***	**#6***	**#7**	**#8**	**#9**	**#10***
SDF-1 alpha	9874	5555	7592	4544	1697	1563	8863	2599	4088	1406
FD-MSC SEC	**#1***	**#2**	**#3**	**#4***	**#5***	**#6**	**#7***	**#8**	**#9**	**#10***
VEGF-A	3446	5663	6634	2434	1138	6323	4874	5394	3245	1034
SDF-1 alpha	2167	4454	5110	1547	1364	5638	2168	3120	2345	1232

Ten MSC samples for each secretome type are shown. Samples excluded from the study are indicated by the asterisk * (VEGF-A and SDF-1 alpha amounts below 2000 pg/ml). Selected secretome batches also undergo *in vitro* cell based assays to assess their biological activity (e.g., real-time cell migration) (data not shown). Concentrations of soluble factors are expressed in pg/ml. Abbreviations: UC, umbilical cord; FD, fetal dermis; sec, secretome.

total of three total applications (Fig. 1C). The study included the following treatments:

- sterile hydrogel, 1 cm^2 in size the first dressing, with a thickness of 0.3–0.5 cm, loaded with sterile culture medium;
- sterile hydrogel, 1 cm^2 in size for the first dressing, with a thickness of 0.3–0.5 cm, loaded with sterile FD-MSC secretome;
- sterile hydrogel, 1 cm^2 in size for the first dressing, with a thickness 0.3–0.5 cm, loaded with sterile UC-MSC secretome.

Sponge sizes for subsequent applications were produced to match the ulcer size (1 × 1 cm for the first application, and 0.5 × 0.5 cm for the second and the third application). The sponges were loaded with 300 μl of secretome for the first application (1 × 1 cm sponge), and 200 μl of secretome for the second and third application (0.5 × 0.5 cm sponge). After curettage, treatments were applied, and the wound area was covered with Tegaderm (3M Health Care; Tegaderm Roll, St Paul, MN, USA), which was changed weekly until wound healing was complete. Wounds were visually inspected daily until the end of the experiments (day 28). Photographs were taken on days 3, 12, 2, and 28 using a Nikon C-Leds camera and X-Entry Alexasoft software. Wound areas were measured using Nis-Elements AR 3.2 software (Nikon Corporation, Tokyo).

2.6. Histology, immunofluorescence and image analysis

At the end of treatments on day 28, mice were sacrificed. Tissue samples were quickly dissected, with left ulcers collected for molecular biology analysis and right ulcers collected for morphological evaluation. For histological examination, samples were fixed in a 4% (w/v) paraformaldehyde solution and picric acid–saturated aqueous solution in 0.1 M Sörensen's phosphate buffer (pH 7.4). Samples were subsequently embedded in paraffin, sectioned at 4 μm thickness, and stained with hematoxylin and eosin (H&E). For immunofluorescence, samples were fixed as described above for 24 h and washed for 48 h in 0.1 M phosphate buffer 5.0% sucrose [14]. After freezing in CO_2, 14 μm thick sections were obtained using a cryostat (HM550 Microm; Bio-Optica, Milan, Italy). These sections were collected on gelatin-coated slides and incubated overnight at 4 °C in a humid chamber with primary antibody anti-laminin (rabbit, 1:150 dilution; R&D Systems). Following 20 min rinsing in PBS, sections were incubated at 37 °C for 30 min in a humid chamber with a secondary antiserum Cy2 Donkey anti-Rabbit IgG (Jackson Immunoresearch) 1:100 diluted in 0.3% Triton/PBS. Subsequently, sections were rinsed in PBS and mounted in glycerol containing 1,4-phenylendiamine (0.1 g/L).

For morphological analysis, five images and two levels per animal, sampled at the center of the repaired ulcer were considered in each animal. All analyses were performed in a blind manner. Epidermal thickness was determined at the equator of the wounded area using H&E staining on histologic sections in the same region. The mean value of five measurements per section and three sections per animal was used for statistical analysis. Immunofluorescence images were captured using a Nikon Eclipse E600 microscope equipped with the Q Imaging Retiga-2000RV digital CCD camera (Q Imaging, Surrey, BC, Canada) and a motorized z-axis stage. Image analysis was performed using the Nis-Elements AR 3.2 software, with the same procedure applied to all images under comparison. The laminin-immunoreactive area was calculated as the area fraction over 400 × 300 μm area and expressed percentage value.

2.7. Gene expression analysis (real-time PCR)

Total RNA was extracted from frozen biopsies, representing half of the ulcer, at the end of the experiment (day 28), using the TissueLyser LT (Qiagen, Hilden, Germany). The extracted total RNA was subsequently purified using the RNAeasy mini kit (Qiagen), quantified and pooled. The expression profile of 168 pathway-related genes in each group was analyzed using the RT2 Profiler PCR mouse arrays specific to angiogenesis (PAMM-024Z), and ECM and adhesion proteins (PAMM-013Z) (Qiagen). The CFX96 real-time PCR system (Bio-Rad Laboratories, Richmond, CA, USA) was employed for this purpose. Relative gene expression was determined using the GeneGlobe online software. The RT2 PCR array plates contain 84 genes associated with the specific pathway and 5 proposed housekeeping genes (*Actb*, *B2m*, *Gapdh*, *Gusb*, *Hsp90ab1*) (supplementary materials S2). Depending on intergroup variability, the *Hsp90ab1* gene was automatically selected by the software for normalization. The plates also included internal controls for genomic DNA contamination, reverse transcription controls, and positive PCR controls. All analyzed plates successfully passed the quality check based on the internal controls.

To further investigate the gene expression profile in healed ulcers treated with the two secretomes, we conducted a separate analysis. This analysis compared the hydrogel + FD-MSC secretome and hydrogel + UC-MSC secretome treated groups with the hydrogel-only group as the control. First, we used GeneGlobe software to perform the comparison, and then we used the differentially regulated genes as input data for pathway enrichment analysis in GeneCodis software (v. 4), employing the mouse genomic informatics (MGI) and KEGG databases.

2.8. Statistical analysis

Data are expressed as mean ± SEM. Data analysis was conducted using Student's t-test or one-way ANOVA, performed with GraphPad Software (San Diego, CA, USA). Results were considered statistically significant when the probability of their occurrence due to chance alone was less than 5% ($p < 0.05$).

3. Results

3.1. Animal monitoring and pain threshold

The animals were monitored daily for dressing integrity, local infection, and general health conditions. During the entire experiment, there were no differences in body weight gain among the groups (Fig. 2A). In addition, all diabetic mice consistently exhibited blood glucose levels above 350 mg/dL and (Fig. 2B).

3.2. Healing of pressure ulcers

Images of representative wounds at various time-points (day 3, 12, 21, and 28) displayed a reduction in skin erythema as early as day 12 in ulcers treated with hydrogel + secretome from both types of MSCs, in comparison to ulcers treated with hydrogel only or the vehicle (Fig. 3A). At the final time point, all the treatments led to a significant reduction in the open wound area when compared to the vehicle group (Fig. 3B). Overall, the residual ulcer areas in the treated groups were smaller than those in the vehicle group. Notably, ulcers treated with hydrogel + secretome from FD-MSCs exhibited a smaller residual de-epithelialized area (Fig. 3C). Evaluation of open ulcers on sacrifice day revealed 5 out of 16 open

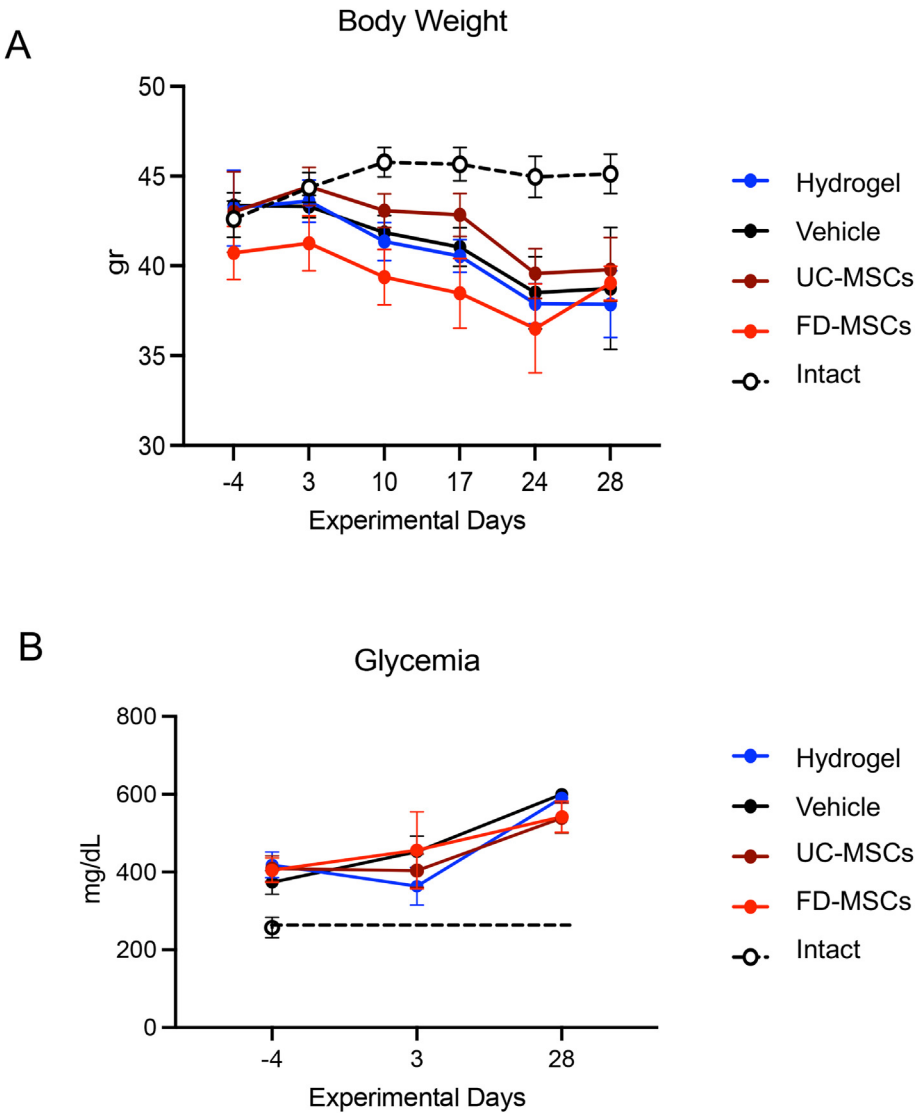

Fig. 2. Animal monitoring. (A) Body weight measurements recorded at regular intervals throughout the experimental timeline. (B) Blood glucose levels measured using Contour XT over the course of study period.

ulcers in the hydrogel + secretome groups, 7 out of 16 open ulcers in the hydrogel-only group, and 15 out of 16 open ulcers in the vehicle group (Fig. 3D).

3.3. Histological analysis: dermal annexes and epidermal thickness

Histological examination of the healed ulcers on day 28 (Fig. 4A and B) revealed a persistent granulation phase in the central area (arrows) in both the vehicle and hydrogel-only treated groups, while skin tissue was largely restored at the periphery of the lesion (Fig. 4A). Notably, the granulation area was smaller in ulcers treated with hydrogel + FD-MSC secretome compared to the other groups. Dermal annexes (asterisks in Fig. 4A) were primarily observed in ulcers treated with hydrogel-only and hydrogel + FD-MSC secretome (Fig. 4A). Histological analysis of the dorsal skin indicated a significantly greater epidermal thickness in ulcers treated with hydrogel + secretome of both MSC types, compared to the vehicle group (Fig. 4C).

3.4. Skin re-vascularization

Vascularization was assessed using laminin-IR immunostaining. Laminin is an integral endothelial basement membrane component widely used as marker for vessels in the skin [37]. The healed skin exhibited a significant increase in capillary density when treated with secretome from both MSC types, compared to the vehicle group (Fig. 5A). The result was further supported by relative quantification of the immunoreactive area (Fig. 5B).

3.5. Gene expression analysis

At the stage of 100% wound closure, treated ulcers exhibited a significant upregulation of genes associated with angiogenesis and ECM (vehicle vs. intact) (supplementary material S2; supplementary figure S1). Specifically, upon analyzing the expression patterns of angiogenesis-related genes, ulcers treated with the hydrogel-only and hydrogel + UC-MSC secretome formed a distinct cluster

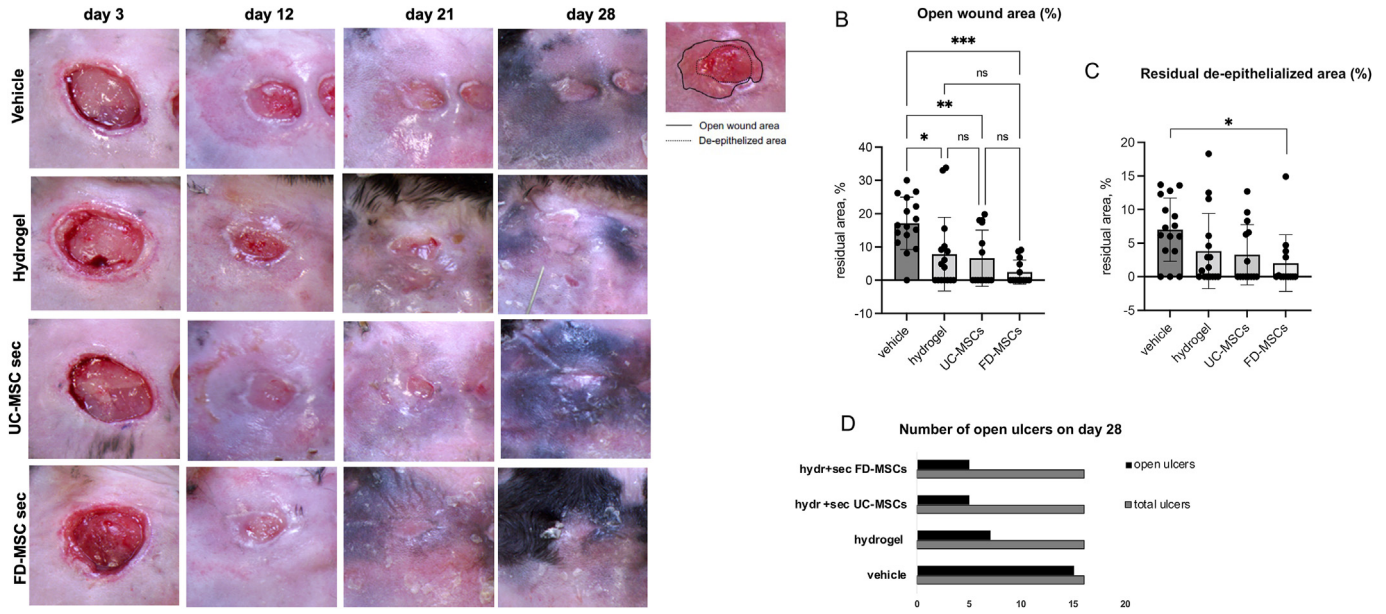

Fig. 3. Pressure ulcer treatment. (A) Representative images of ulcers taken on days 3, 12, 21, and 28 post-lesion. A noticeable reduction in skin erythema is observed as early as day 12 in hydrogel + secretome-treated ulcers compared to the vehicle and hydrogel-only-treated ulcers. (B) Open wound area on day 28 expressed as a percentage of the ulcer area on day 3. (C) Residual de-epithelialized area on day 28 vs. day 3. (D) Number of open ulcers at the end of the experiment. Statistical significance was determined using one-way ANOVA and Tukey's post-hoc test for treatment vs. vehicle group (*p < 0.05; **p < 0.01; ***p < 0.001). UC, umbilical cord; FD, fetal dermis; sec, secretome.

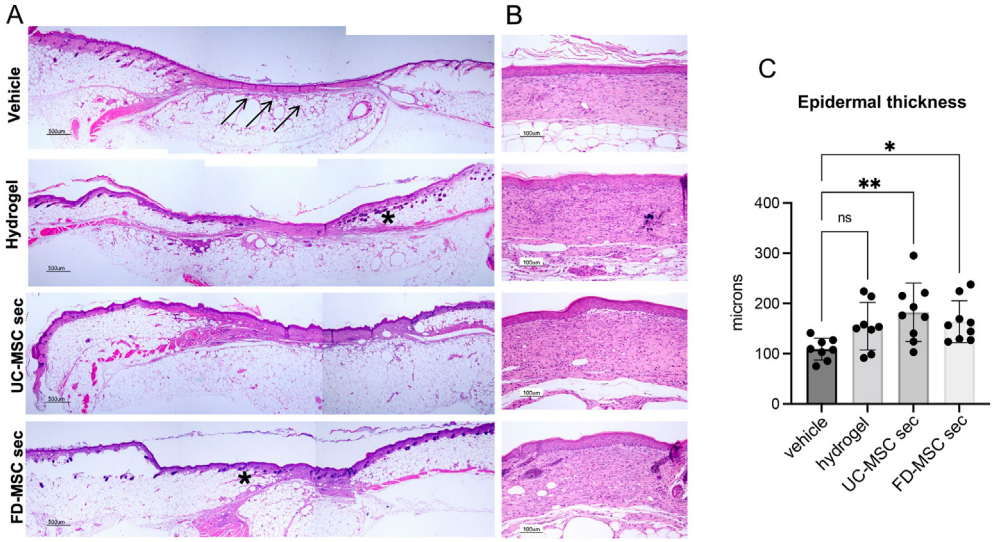

Fig. 4. Histological analysis of repaired ulcers on day 28. (A) Representative micrographs of H&E-stained sections showing vehicle and treated ulcers at the lesion equator at low magnification. Arrows indicate the presence of a granulation phase in the central area of the lesion. (B) The same micrographs at high magnification. (C) Morphometric evaluation of epidermal thickness measured at wound closure. Statistical significance was determined using one-way ANOVA and Dunnet's post-hoc test for treatment vs. vehicle group (*p < 0.05; **p < 0.01). UC, umbilical cord; FD, fetal dermis; sec, secretome. Scale bars: 500 μm (A); 100 μm (B).

(cluster 1), which was separate from cluster 2 consisting of ulcers treated with the vehicle and ulcers treated with hydrogel + FD-MSC secretome. The intact tissue group occupied an intermediate position between the two clusters, forming a sub-cluster within cluster 1 (Fig. 6A). Using the vehicle-treated ulcers as the normalizer group, the hydrogel-only group exhibited significant overexpression of three genes (*Cxcl1*, *Il6*, *Mmp9*; fold change ≥3). Notably, *CXCL1* and *IL6* genes displayed similar overexpression in the hydrogel + FD-MSC secretome group, along with *Csf3*, *Cxcl5*, *Mmp9*, and *Serpine1*. In contrast, the hydrogel + UC-MSC secretome group displayed differential expression in only one gene (*Ifng*), which was downregulated (Fig. 6A).

Upon analyzing the expression pattern of ECM-related genes, the hydrogel + UC-MSC secretome and hydrogel + FD-MSC-secretome groups formed separate clusters, while the vehicle, the hydrogel-only and intact groups represented different subclusters (Fig. 6B). Using the vehicle group as the normalizer group, the hydrogel-only group exhibited the most altered gene expression pattern, with seven significantly overexpressed genes (*Cd44, Mmp3, Mmp8, Mmp9, Mmp10, Mmp13*, and *Tnc*; fold change ≥3). Similar to the angiogenesis-related genes, the hydrogel + FD-MSC secretome group shared overexpressed ECM-related genes with the hydrogel-only group (*Mmp3, Mmp8, Mmp10*, and *Tnc*). In addition, the hydrogel + FD-MSC secretome group upregulated the *Sele* gene

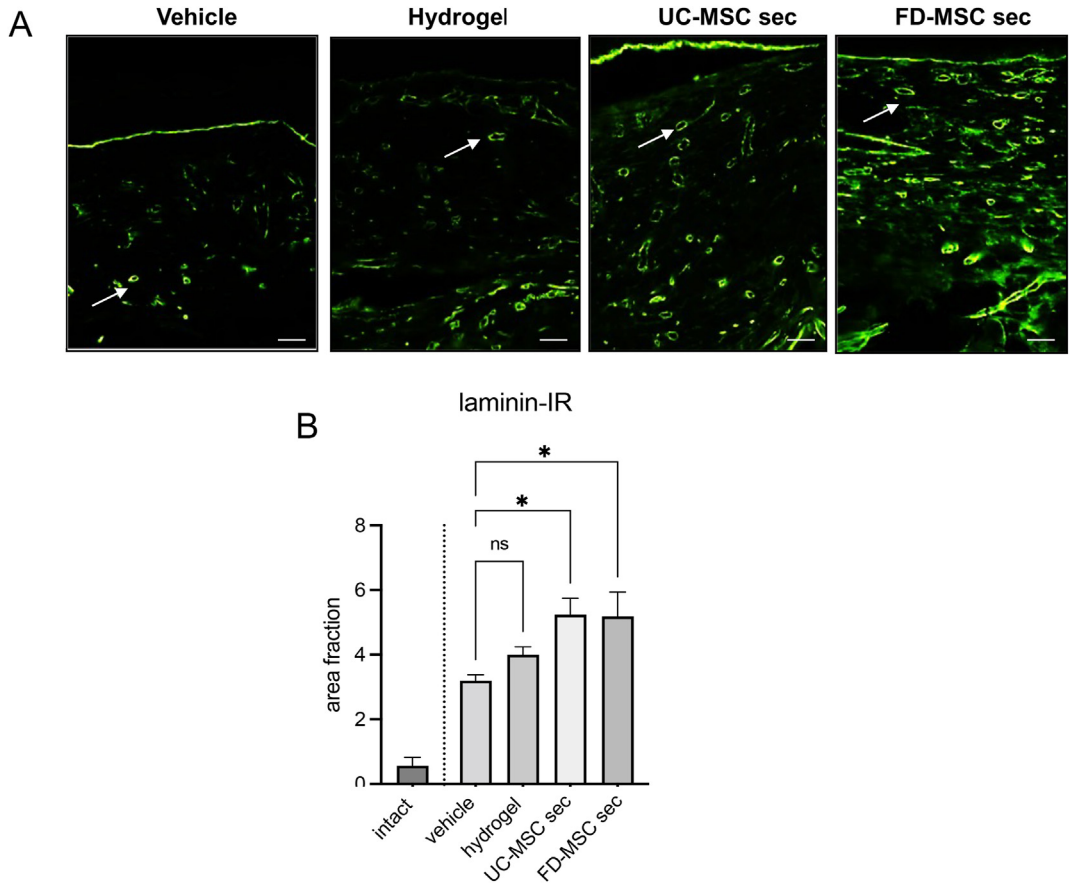

Fig. 5. Skin re-vascularization analyzed by laminin-IR immunofluorescence. (A) Representative micrographs showing vehicle and treated ulcers at the lesion equator. (B) Morphometric assessment of laminin-IR expression presented as the immunoreactive area fraction (capillary density). Statistical significance was determined using one-way ANOVA and Dunnet's post-hoc test for treatment vs. vehicle group (*p < 0.05). UC, umbilical cord; FD, fetal dermis; sec, secretome. Scale bars: 100 μm.

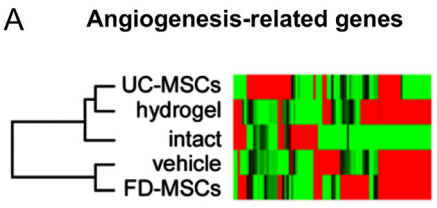

	hydrogel	FD-MSCs	UC-MSCs
Csf3		7.97	
Cxcl1	7.95	3.99	
Cxcl5		4.00	
Ifng			-3.97
Il6	4.00	7.94	
Mmp9	4.01		
Serpine1		4.03	

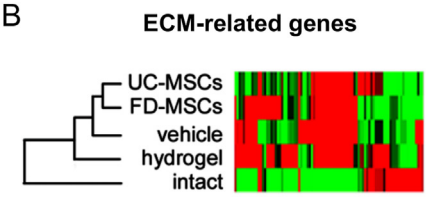

	hydrogel	FD-MSCs	UC-MSCs
Cd44	3.78		
Mmp3	4.01	3.99	
Mmp8	3.99	8.01	
Mmp9	3.99		
Mmp10	16.01	32.07	
Mmp12			-3.98
Mmp13	3.97		
Sele		4.02	
Spp1			-4.00
Tnc	4.02	4.00	

Fig. 6. Gene expression analysis focusing on angiogenesis and ECM-related pathways. (A) Clustergram resulting from the analysis of RT2 PCR angiogenesis array. (B) Clustergram generated by the analysis of RT2 PCR ECM and adhesion molecules array. Each clustergram is accompanied by a table listing the differentially expressed genes (fold change ≥ ± 3) observed in ulcers treated with hydrogel only, hydrogel + FD-MSC secretome, and hydrogel + UC-MSC secretome, compared to the vehicle group. UC, umbilical cord; FD, fetal dermis; MSCs, mesenchymal stromal cells; ECM, extracellular matrix.

compared to the vehicle group. The hydrogel + UC-MSC secretome group showed only two differentially expressed genes (*Mmp12* and *Spp1*), which were both downregulated compared to the vehicle group (Fig. 6B).

To further investigate the impact of the secretome on the healing effect of the hydrogel, we analyzed the molecular profile of the healed ulcers and compared the gene expression profile of ulcers treated with the two MSC secretomes with that of ulcers

treated with the hydrogel-only. For angiogenesis-related genes, the presence of FD-MSC secretome induced upregulation of *Csf3* and *Plau*, while the presence of UC-MSC secretome resulted in downregulation of *Csf3*, *Cxcl5*, *Il6*, and *Mmp9* (Fig. 7A). For ECM-related genes, the FD-MSC secretome did not alter gene expression, while the presence of UC-MSC secretome caused downregulation of several genes (*Mmp10*, *Mmp13*, *Mmp3*, *Mmp9*, and *Tnc*) (Fig. 7B). Then, we used the downregulated genes from the hydrogel + UC-MSC secretome group, compared to the hydrogel-only group, as input data for pathway enrichment analysis (GenCodis v4), using MGI and KEGG reference databases. Notably, we found that these genes are involved in delayed wound healing and abnormal inflammation response (such as abnormal neutrophil physiology and increased susceptibility to bacterial infection), involving the activation of IL17 and TNF pathways, along with proinflammatory pathways (e.g., rheumatoid arthritis) (Fig. 7C). The main identified pathways from the enrichment analysis are listed in supplementary material S3.

3.6. Proteomic profiling of MSC secretome

A detailed proteomic analysis of the two secretomes was conducted to explore potential differences that might have elicited distinct gene expression patterns. High-resolution proteomics identified 457 proteins in UC-MSC secretome and 757 in FD-MSC secretome (supplementary material S4). Among the proteins identified in UC-MSC secretome, 139 were annotated as secreted (UniProt annotation), while 42 proteins were annotated as transmembrane. This latter group included proteins released from the cell membrane through proteolytic processes, while the remaining proteins were annotated as intracellular and included proteins without a signal peptide, proteins associated with exosomes, and others [32]. Finally, 56 proteins were ECM-related proteins (Fig. 8A). The analysis of FD-MSC secretome identified 189 proteins annotated as secreted, 56 as transmembrane, and 69 as ECM-related proteins (Fig. 8A) (supplementary material S4). A total of 312 proteins were shared by both secretomes, while 32 proteins were exclusively found in UC-MSC secretome, and 326 proteins were exclusively found in secretome of FD-MSCs (Fig. 8B). First, we used the GO Enrichr web server to identify proteins present in both secretomes associated with specific molecular pathways and biological processes. The GO-Pathway analysis found that the predominant group of proteins in secretomes of FD-MSCs and UC-MSCs were associated with the VEGFA-VEGFR2 pathway, which is crucial in tissue repair by inducing vascular permeability, recruitment of inflammatory cells to the site of injury, and angiogenesis

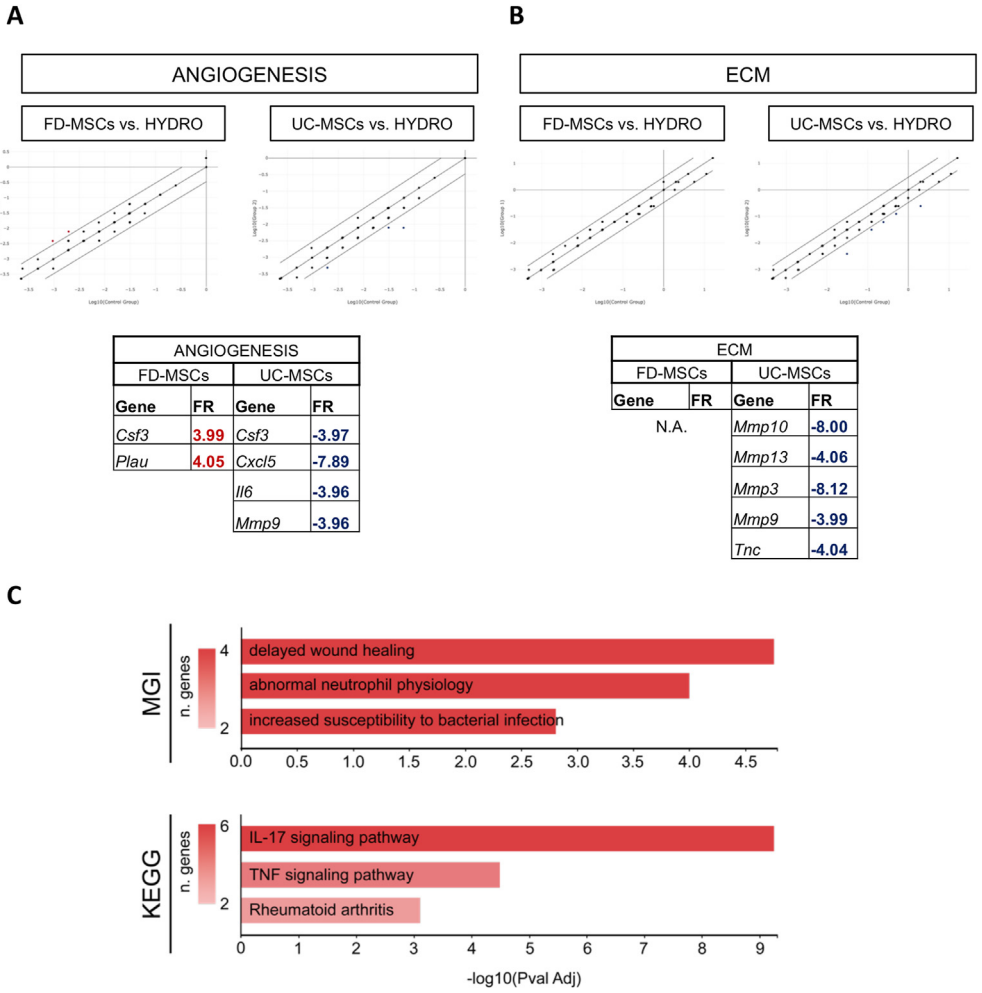

ANGIOGENESIS			
FD-MSCs		UC-MSCs	
Gene	FR	Gene	FR
Csf3	3.99	*Csf3*	-3.97
Plau	4.05	*Cxcl5*	-7.89
		Il6	-3.96
		Mmp9	-3.96

ECM			
FD-MSCs		UC-MSCs	
Gene	FR	Gene	FR
N.A.		*Mmp10*	-8.00
		Mmp13	-4.06
		Mmp3	-8.12
		Mmp9	-3.99
		Tnc	-4.04

Fig. 7. Gene expression regulation induced by hydrogel + secretome treatments compared to hydrogel-only. (A, B) Scatterplot graphs representing the regulation of gene expression related to angiogenesis (A) and ECM (B) in the presence of secretome. Each graph included a list of differentially expressed genes (fold change ≥ ± 3) observed in ulcers treated with hydrogel + FD-MSC secretome and hydrogel + UC-MSC secretome, compared to hydrogel-only. (C) Pathway enrichment analysis of downregulated genes in ulcers treated with hydrogel + UC-MSC secretome compared to hydrogel-only, using the MGI and KEGG databases. UC, umbilical cord; FD, fetal dermis; FR, fold regulation; MSCs, mesenchymal stromal cells; ECM, extracellular matrix; MGI, mouse genomic informatics.

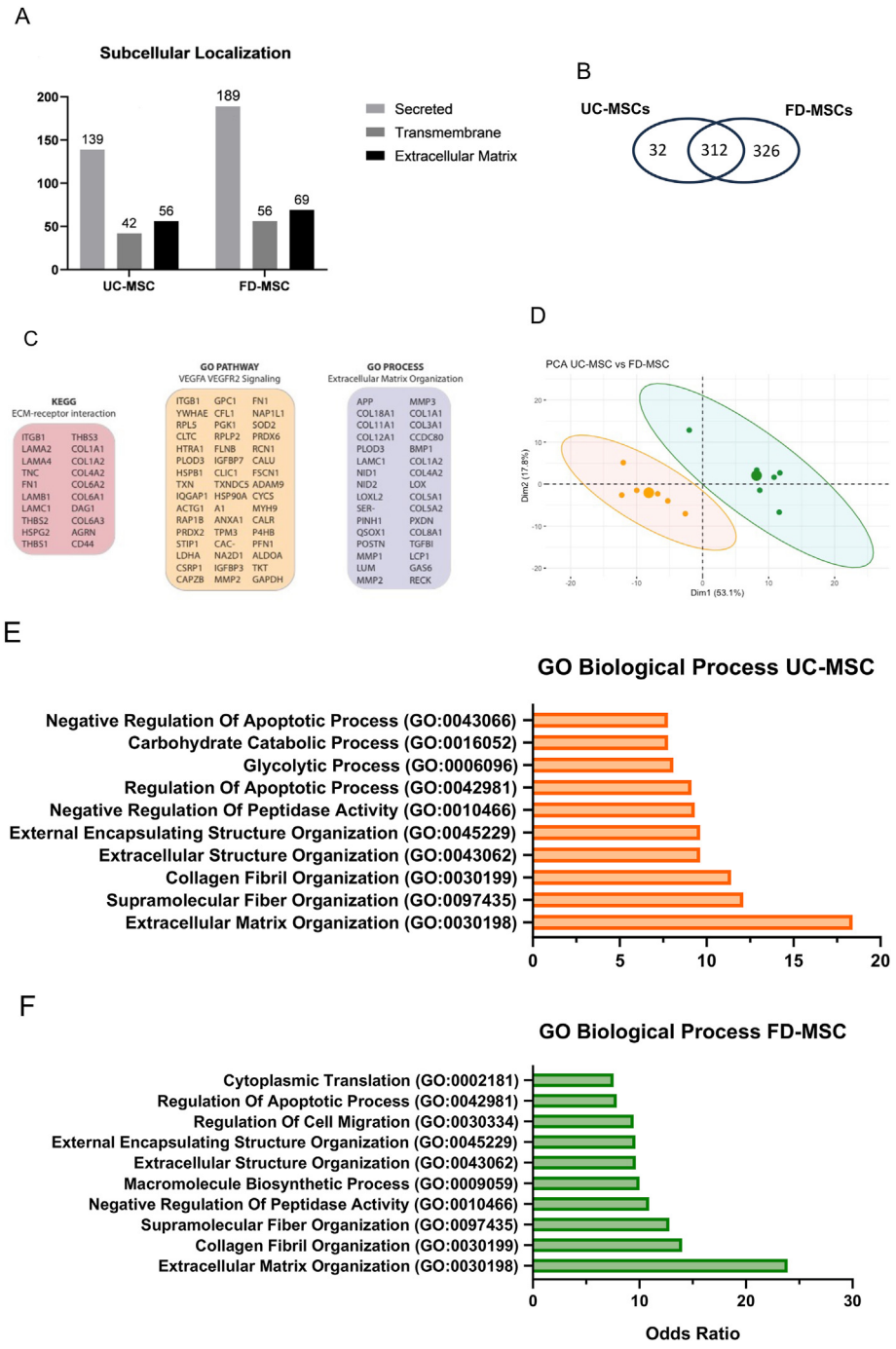

Fig. 8. Proteome profiling of FD-MSC and UC-MSC secretomes. (A) Number and subcellular location of the identified proteins indicating secreted, transmembrane, and ECM-related proteins in UC-MSC and FD-MSC secretomes. The results are based on UniProt annotations. (B) Venn diagram illustrating shared and exclusive proteins identified in both secretomes. (C) List of proteins shared by UC-MSC and FD-MSC secretomes, along with their KEGG and GO annotations. (D) PCA of Z-scored LFQ intensity of the proteins identified in UC-MSC and FD-MSC secretomes. Annotation of the most regulated GOBP among all identified proteins in UC-MSC (E) and FD-MSC (F) secretomes. UC, umbilical cord; FD, fetal dermis; ECM, extracellular matrix; KEGG, Kyoto Encyclopedia of Genes and Genomes; GO, Gene Ontology; PCA, principal component analysis; GOBP, Gene Ontology Biological Processes.

(ISSN 1087−0024) (Fig. 8C; Table 2). Both KEGG and GOBP analysis evidenced a significant association of proteins present in both secretome with ECM organization and ECM-receptor interactions (Fig. 8C; Table 2).

Despite the high number of shared proteins, principal component analysis (PCA) revealed distinct clustering of the two secretomes, indicating significant differences in their composition (Fig. 8D). Thus, we used LFQ to measure the relative abundance of proteins in secretomes of UC-MSCs and FD-MSCs and analyzed such differences in protein composition. In addition to the proteins exclusively found in either UC-MSCs or FD-MSCs secretomes, for which GOBP analysis revealed a similar association with ECM organization (Fig. 8E and F), LFQ revealed 234 proteins exhibiting differential abundance between the two secretomes. Among these, 40 proteins were more abundant in UC-MSC secretome (Fig. 9A; Table 3), while 194 proteins were more abundant in FD-MSC

Table 2
List of the most enriched terms in the GO pathways, biological process and KEGG analysis.

GO pathway analysis				
Term	Overlap	p-value	Adjusted p-value	Proteins
VEGFA VEGFR2 Signaling WP3888	47/430	3,03E-08	1,10E-05	ITGB1; YWHAE; RPL5; CLTC; HTRA1; PLOD3; HSPB1; TXN; IQGAP1; ACTG1; RAP1B; PRDX2; STIP1; LDHA; CSRP1; CAPZB; GPC1; CFL1; PGK1; RPLP2; FLNB; IGFBP7; CLIC1; TXNDC5; HSP90AA1; ANXA1; TPM3; CACNA2D1; IGFBP3; MMP2; FN1; NAP1L1; SOD2; PRDX6; RCN1; CALU; FSCN1; ADAM9; CYCS; MYH9; CALR; P4HB; PFN1; ALDOA; TKT; GAPDH; VCL
KEGG analysis				
Term	Overlap	p-value	Adjusted p-value	Proteins
ECM-receptor interaction	20/88	3,33E-02	7,06E+01	ITGB1; LAMA2; LAMA4; TNC; FN1; LAMB1; LAMC1; THBS2; HSPG2; THBS1; THBS3; COL1A1; COL1A2; COL4A2; COL6A2; COL6A1; DAG1; COL6A3; AGRN; CD44
GO Biological Processes analysis				
Term	Overlap	p-value	Adjusted p-value	Proteins
Extracellular Matrix Organization (GO:0030198)	31/176	1,79E-06	3,95E-03	APP; COL18A1; COL11A1; COL12A1; PLOD3; LAMC1; NID1; NID2; LOXL2; SERPINH1; QSOX1; POSTN; MMP1; LUM; MMP2; MMP3; COL1A1; COL3A1; CCDC80; BMP1; COL1A2; COL4A2; LOX; COL5A1; COL5A2; PXDN; COL8A1; TGFBI; LCP1; GAS6; RECK

Table displaying term names, overlap, p-values, adjusted p-values, and proteins (by gene names) associated with terms in the GO or KEGG analysis. The most enriched terms for each analysis are listed.

secretome (Fig. 9A; Table 4). GOBP analysis of proteins more abundant in FD-MSC secretome revealed enrichments in supermolecular fiber organization (GO:0097435) and regulation of basement membrane organization (GO:0110011), along with additional processes (Fig. 9B). In contrast, GOBP analysis of proteins more abundant in UC-MSC secretome revealed enrichments in

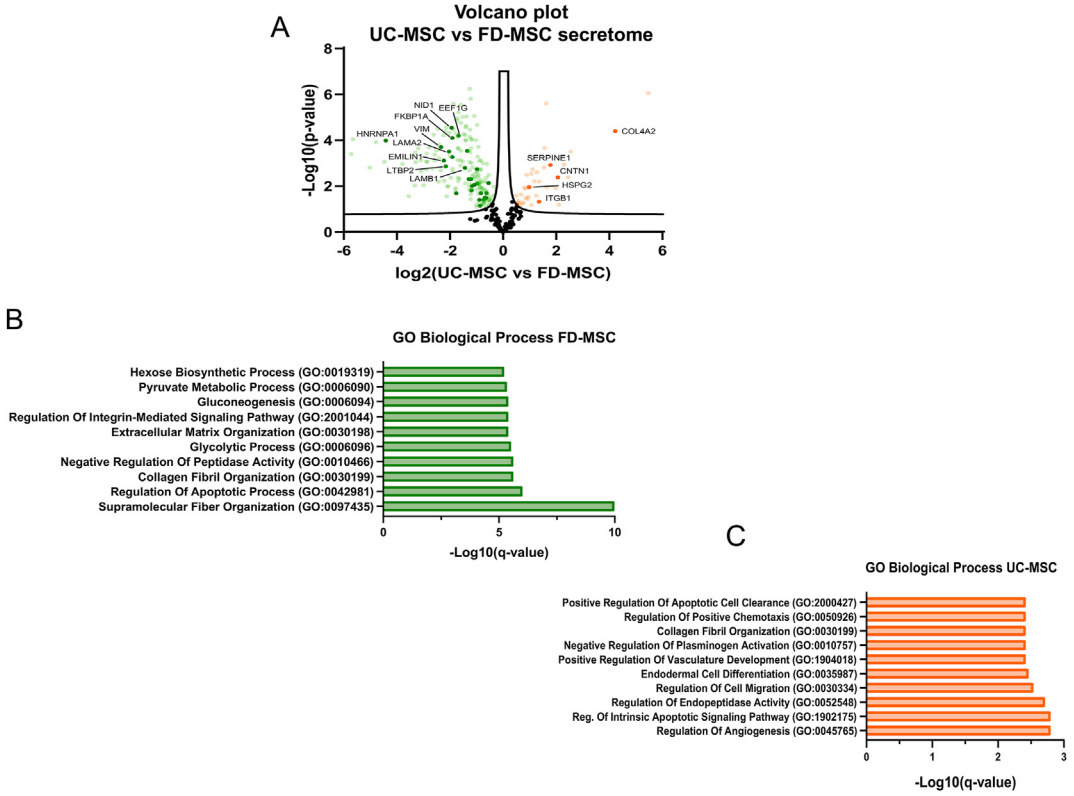

Fig. 9. Identification of differentially abundant proteins in secretomes of UC-MSCs and FD-MSCs. (A) Volcano plot showing 312 shared proteins among the two secretomes. The $\log_2$ ratio between protein abundance in secretome of the two MSC sources (UC-MSC/FD-MSC) was plotted against the $\log_{10}$ of the *p*-value. Proteins above the FDR, indicated by black dashed lines, achieved statistical significance. Proteins highlighted in green and orange solid points represent the two most regulated annotations according to the GOBP database ($n = 6$). Bar graph plot showing the $\log_{10}$ of the q-value of the TOP10 GOBP categories identified among the differentially abundant proteins in FD-MSC (B), and UC-MSC (C) secretomes. UC, umbilical cord; FD, fetal dermal; MSC, mesenchymal stromal cells; FDR, false discovery rates; GOBP, Gene Ontology Biological Processes.

Table 3
Selected proteins significantly abundant in UC-MSC secretome.

Protein names	Gene names	Protein IDs	Fold change	-Log10 (p-value)
Carboxypeptidase A4	*CPA4*	Q9UI42	5,467874908	6,064,019,703
Collagen alpha-2(IV) chain	*COL4A2*	P08572	4,222,429,911	4,401,915,533
Insulin-like growth factor-binding protein 7	*IGFBP7*	Q16270	2,54,617,048	3,506,769,477
Insulin-like growth factor-binding protein 5	*IGFBP5*	P24593	2,446,849,251	2,382,357,839
Lactadherin	*MFGE8*	Q08431	2,29,502,449	2,943,068,379
Inhibin beta A chain	*INHBA*	P08476	2,101,693,108	1,187,562,729
Contactin-1	*CNTN1*	Q12860	2,063,464,791	2,382,478,893
Lysyl oxidase homolog 2	*LOXL2*	Q9Y4K0	1,982,924,816	1,918,693,722
Plasminogen activator inhibitor 1	*SERPINE1*	P05121	1,786,638,968	2,925,709,911
Testican-1	*SPOCK1*	Q08629	1,65,281,601	1,943,222,957
Cadherin-2	*CDH2*	P19022	1,621,836,408	5,607,843,194
60 kDa heat shock protein	*HSPD1*	P10809	1,564,852,905	3,669,422,191
Galectin-3-binding protein	*LGALS3BP*	Q08380	1,537,068,231	2,815,564,622
Collagen alpha-1(XI) chain	*COL11A1*	P12107	1,360,860,189	2,204,441,527

Protein name: abundant proteins in UC-MSC secretome. Gene name: Uniprot gene name associated with each protein. Protein ID: UniProt accession number of the protein. Fold change: log2 transformed ratio between the mean of LFQ values of FD-MSCs and UC-MSCs (n = 3). -Log10 (p-value): for three biological replicates.

Table 4
Selected proteins significantly abundant in FD-MSC secretome.

Protein names	Gene names	Protein IDs	Log2 (FD-MSC/UC-MSC)	-Log10 (p-value)
Adipocyte enhancer-binding protein 1	*AEBP1*	Q8IUX7	−5,7,153,472	3,4,078,516
Lamin-A/C	*LMNA*	P02545;	−5,6,516,198	4,04,565,156
Interstitial collagenase	*MMP1*	P03956	−5,0179429	2,81,835,814
Plectin	*PLEC*	Q15149	−4,7,923,747	3,92,567,839
Pigment epithelium-derived factor	*SERPINF1*	P36955	−4,4,675,045	3,0726229
Heterogeneous nuclear ribonucleoprotein A1	*HNRNPA1*	F8W6I7	−4,4,172,305	3,99,261,563
Clusterin	*CLU*	P10909	−3,7,896,061	2,96,780,353
Stromelysin-1	*MMP3*	P08254	−3,5,518,073	1,5,624,198
Fibrillin-2	*FBN2*	P35556	−3,3,238,164	2,03,233,106
Collagen alpha-3(VI) chain	*COL6A3*	P12111;	−3,3,018,936	3,46,097,394
CD109 antigen	*CD109*	Q6YHK3	−3,2,923,721	3,04,126,895
Collagen alpha-2(VI) chain	*COL6A2*	P12110	−3,1,962,757	3,6,496,932
Clathrin heavy chain; Clathrin heavy chain 1	*CLTC*	A0A087WVQ6	−3,1,052,525	3,12,867,301
Complement C1r subcomponent	*C1R*	A0A3B3ISR2	−3,0859991	2,65,950,717
Peptidyl-glycine alpha-amidating monooxygenase	*PAM*	P19021	−2,9,869,562	2,04,572,642

Protein name: abundant proteins in FD-MSC secretome. Gene name: Uniprot gene name associated with each protein. Protein ID: UniProt accession number of the protein. Fold change: log2 transformed ratio between the mean of LFQ values of FD-MSCs and UC-MSCs (n = 3). -Log10 (p-value): for three biological replicates.

regulation of angiogenesis (GO:0045765) and negative regulation of plasminogen activation (GO:0010757) processes (Fig. 9C) (supplementary material S4).

4. Discussion

Our previous *in vitro* studies of collection and characterization of secretome from various MSC sources, laid the essential framework for upcoming *in vivo* investigations assessing the efficacy of secretome-based therapy. These studies included the establishment of standardized collection procedures, quantification of secretome bioactive factors, and assessment of secretome ability to stimulate cellular responses relevant to tissue repair, such as cell migration, proliferation, and angiogenesis [29,30,38–40]. In this context, we set cut-off values (i.e., significant cytokine contents and biological activities) to carefully select samples considered suitable for preparing secretome batches for subsequent *in vivo* studies. This selection has proven particularly relevant, given the considerable variability in secretome composition and biological activity associated with donor variabilities [41].

A strategy in secretome-based therapy involves developing polymeric combination products capable to sustain the delivery of secretome at the wound site [42]. Given their ability to sequester therapeutically active compounds and regulate their release, HA-based hydrogels are deemed suitable for secretome delivery. In previous studies, we described the synthesis procedure of a chemically modified HA derivative, produced in the form of dried sponges [27,43]. Upon rehydration with secretome, these sponges formed a hydrogel capable of sustaining secretome release [28]. The findings from release kinetics studies guided the design of the treatment schedule in the present study, involving one hydrogel application every 9 days over a 28-day period, with a total of three applications. Our device was specifically designed to combine hydrogel and cellular properties. The hydrogel ensures a prolonged release of cell-derived growth factors and cytokines [28], while the secretome regulates cellular and molecular processes essential for wound repair, including re-epithelization, cell migration, ECM deposition, angiogenesis, and scar reabsorption. Recently, we demonstrated that incorporating a specific integrin ligand ($\alpha4\beta1$ integrin target) into a PLGA-based medication alters the molecular profile of treated skin towards a non-fibrotic state [44].

The prolonged inflammatory phase and impaired vascularization in the ulcers of the db/db mouse render this model particularly suitable for assessing the MSC secretome as a pro-healing agent [45]. At the halfway point of the repair process, visual observations evidenced a reduced skin erythema only in ulcers treated with the hydrogel + secretome combination. Both the hydrogel only and hydrogel + secretome were equally effective in enhancing wound closure. The observed pro-heling effect of the hydrogel raises the longstanding question of whether HA should be regarded as a drug, considering its anti-inflammatory and reparatory effects [46]. However, the presence of secretome was crucial to enhance the intrinsic healing properties of HA. Of particular significance is the

increased microcirculation within the healed area, holding promise for diabetic ulcer treatment [47,48].

Both UC-MSC and FD-MSC secretomes demonstrated comparable efficacy in promoting ulcer healing. The proteomic profiles of both secretomes support this observation, as evidenced by the number of shared proteins enriching various tissue repair-related pathways and biological processes, including angiogenesis and ECM remodeling. These finding are in agreement with the previous hypothesis of a common secreted protein signature responsible for the MSC therapeutic effect, despite variations in sources and isolation methods [49].

Despite the similar efficacy and composition of the two secretomes, gene expression analysis performed on healed ulcers revealed a distinct pattern of the hydrogel + UC-MSC secretome treatment compared to the other treatments. Notably, the hydrogel-only and hydrogel + FD-MSC secretome treatments induced upregulation of wound healing genes such as *IL6* [50] and *Mmp10*, which are known to support cell migration at the wound edge [51]. Additionally, the hydrogel + FD-MSC secretome treatment strongly stimulated the expression of the *Csf3* gene encoding Granulocyte-Colony Stimulating Factor (G-CSF), a chemokine known to accelerate wound healing by enhancing angiogenesis, which has also been tested in clinical trials [52]. Interestingly, UC-MSC secretome appeared to counteract the hydrogel-induced upregulation of *MMP* genes. Given the detrimental impact of high MMP levels on chronic wound healing [51,53], this effect may enhance wound healing by promoting a more balanced expression of key regulatory factors involved in tissue repair and remodeling. The ability of UC-MSC secretome to modulate the expression of MMP genes may be attributed to the differential abundance of proteins compared to FD-MSC secretome. These proteins enrich the GOBP "negative regulation of plasminogen activation" (GO:001057). Considering that plasminogen is an activator of MMP secretion [54], this enrichment suggests the existence of a regulatory mechanism mitigating the hydrogel-induced effects.

Comparing the molecular signature of ulcers treated with secretome + hydrogel to those treated with the hydrogel-only highlighted significant differences between these treatments. Notably, the presence of secretomes induces a differential expression of genes involved in angiogenesis and ECM regulation. KEGG- and MGI-based enrichment analysis using the GeneGlobe software identifies the most represented pathways among the differentially regulated gene. This analysis indicates that incorporating MSC secretome into the hydrogel downregulates genes that delay wound healing and activate an abnormal inflammatory response.

5. Conclusions

Our cell-free approach for diabetic ulcer treatment relies on the inherent anti-inflammatory and pro-regenerative properties of MSC secretome. The findings emphasize the capacity of MSC secretome to coordinate wound healing processes, even in the presence of systemic diseases such as diabetes. The results also support the healing effect of the HA hydrogel, with MSC secretome amplifying its therapeutic action. The procedure is user-friendly, allowing for the preparation of frozen batches that can be shipped as ready-to-use products. This approach offers advantages over cellular skin substitutes, which require a high level of expertise in cell manufacturing. Additionally, our approach may mitigate the significant drawback of low engraftment rates commonly associated with skin substitutes. The HA hydrogel + secretome device holds potential for advancing the field of chronic skin wound management. Further preclinical investigations are necessary to fully harness the device's potential and validate the efficacy of the treatment.

Credit authorship contribution statement

Fabio Salvatore Palumbo: methodology, data curation. **Matteo Calligaris**: data curation, validation, writing. **Laura Calzà**: resources, supervision, manuscript writing, review & editing. **Calogero Fiorica**: methodology, data curation**. Vito Antonio Baldassarro**: methodology, data curation and writing. **Anna Paola Carreca**: methodology. **Luca Lorenzini**: data curation, formal analysis, software, validation. **Alessandro Giuliani**: data curation, formal analysis, software, validation. **Claudia Carcione**: methodology, data curation. **Nicola Cuscino:** data curation. **Giovanna Pitarresi**: methodology, data curation. **Simone Dario Scilabra**: data curation, validation, writing. **Pier Giulio Conaldi**: funding acquisition, supervision. **Cinzia Maria Chinnici**: conceptualization, writing original draft, supervision, review & editing.

Declaration of competing interest

The authors declare the following financial interests/personal relationships which may be considered as potential competing interests: Pier Giulio Conaldi reports financial support was provided by Sicilian Region. Cinzia Chinnici has patent #102023000019479 pending to ISMETT and Ri.MED. If there are other authors, they declare that they have no known competing financial interests or personal relationships that could have appeared to influence the work reported in this paper.

Acknowledgements

The authors wish to thank the Gynecology Unit (Ospedale Civico, Palermo) for providing the human fetal skin biopsies. This research was funded by PO FESR Sicilia 2014/2020 Azione 1.1.5. Project 08PA8610200270 "Prometeo".

Appendix A. Supplementary data

Supplementary data to this article can be found online at https://doi.org/10.1016/j.reth.2024.07.008.

References

[1] Frykberg RG, Banks J. Challenges in the treatment of chronic wounds. Adv Wound Care 2015;4:560–82. https://doi.org/10.1089/WOUND.2015.0635.
[2] Baldassarro VA, Lorenzini L, Giuliani A, Cescatti M, Alastra G, Pannella M, et al. Molecular mechanisms of skin wound healing in non-diabetic and diabetic mice in excision and pressure experimental wounds. Cell Tissue Res 2022;388:595–613. https://doi.org/10.1007/S00441-022-03624-X.
[3] Niezgoda JA, Van Gils CC, Frykberg RG, Hodde JP. Randomized clinical trial comparing OASIS Wound Matrix to Regranex Gel for diabetic ulcers. Adv Skin Wound Care 2005;18:258–66. https://doi.org/10.1097/00129334-200506000-00012.
[4] Lebrun E, Tomic-Canic M, Kirsner RS. The role of surgical debridement in healing of diabetic foot ulcers. Wound Repair Regen 2010;18:433–8. https://doi.org/10.1111/J.1524-475X.2010.00619.X.
[5] Kolimi P, Narala S, Nyavanandi D, Youssef AAA, Dudhipala N. Innovative treatment strategies to accelerate wound healing: trajectory and recent advancements. Cells 2022;11. https://doi.org/10.3390/CELLS11152439.
[6] Guo S, DiPietro LA. Factors affecting wound healing. J Dent Res 2010;89:219–29. https://doi.org/10.1177/0022034509359125.
[7] Tran C, Damaser MS. Stem cells as drug delivery methods: application of stem cell secretome for regeneration. Adv Drug Deliv Rev 2015;82–83:1–11. https://doi.org/10.1016/J.ADDR.2014.10.007.
[8] Ahangar P, Mills SJ, Cowin AJ. Mesenchymal stem cell secretome as an emerging cell-free alternative for improving wound repair. Int J Mol Sci 2020;21:1–15. https://doi.org/10.3390/IJMS21197038.
[9] Xia J, Minamino S, Kuwabara K, Arai S. Stem cell secretome as a new booster for regenerative medicine. Biosci Trends 2019;13:299–307. https://doi.org/10.5582/BST.2019.01226.
[10] Mesenchymal stem cell-derived pleiotropic factor in treating non-healing wounds - full text view - ClinicalTrials.gov n.d. https://classic.clinicaltrials.gov/ct2/show/NCT04235868. [Accessed 2 February 2024].

[11] Therapeutic potential of stem cell conditioned medium on chronic ulcer wounds - full text view - ClinicalTrials.gov n.d. https://classic.clinicaltrials.gov/ct2/show/NCT04134676. [Accessed 2 February 2024].
[12] Alpers CE, Hudkins KL. Mouse models of diabetic nephropathy. Curr Opin Nephrol Hypertens 2011;20:278–84. https://doi.org/10.1097/MNH.0B013E3283451901.
[13] Sullivan SR, Underwood RA, Gibran NS, Sigle RO, Usui ML, Carter WG, et al. Validation of a model for the study of multiple wounds in the diabetic mouse (db/db). Plast Reconstr Surg 2004;113:953–60. https://doi.org/10.1097/01.PRS.0000105044.03230.F4.
[14] Giuliani A, Lorenzini L, Baldassarro VA, Pannella M, Cescatti M, Fernandez M, et al. Effects of topical application of CHF6467, a mutated form of human nerve growth factor, on skin wound healing in diabetic mice. J Pharmacol Exp Therapeut 2020;375:317–31. https://doi.org/10.1124/JPET.120.000110.
[15] Pitarresi G, Palumbo FS, Triolo D, Fiorica C, Giammona G. A methacrylic hyaluronic acid derivative for potential application in oral treatment of celiac disease. Drug Dev Ind Pharm 2017;43:1480–8. https://doi.org/10.1080/03639045.2017.1319380.
[16] Palumbo FS, Fiorica C, Di Stefano M, Pitarresi G, Gulino A, Agnello S, et al. In situ forming hydrogels of hyaluronic acid and inulin derivatives for cartilage regeneration. Carbohydr Polym 2015;122:408–16. https://doi.org/10.1016/J.CARBPOL.2014.11.002.
[17] Tavianatou AG, Caon I, Franchi M, Piperigkou Z, Galesso D, Karamanos NK. Hyaluronan: molecular size-dependent signaling and biological functions in inflammation and cancer. FEBS J 2019;286:2883–908. https://doi.org/10.1111/FEBS.14777.
[18] Abatangelo G, Vindigni V, Avruscio G, Pandis L, Brun P. Hyaluronic acid: redefining its role. Cells 2020;9:1–19. https://doi.org/10.3390/CELLS9071743.
[19] Hussain Z, Pandey M, Thu HE, Kaur T, Jia GW, Ying PC, et al. Hyaluronic acid functionalization improves dermal targeting of polymeric nanoparticles for management of burn wounds: in vitro, ex vivo and in vivo evaluations. Biomed Pharmacother 2022;150. https://doi.org/10.1016/J.BIOPHA.2022.112992.
[20] Abednejad A, Ghaee A, Nourmohammadi J, Mehrizi AA. Hyaluronic acid/carboxylated Zeolitic Imidazolate Framework film with improved mechanical and antibacterial properties. Carbohydr Polym 2019;222. https://doi.org/10.1016/J.CARBPOL.2019.115033.
[21] Kawano Y, Patrulea V, Sublet E, Borchard G, Iyoda T, Kageyama R, et al. Wound healing promotion by hyaluronic acid: effect of molecular weight on gene expression and in vivo wound closure. Pharmaceuticals 2021;14. https://doi.org/10.3390/PH14040301.
[22] Li X, Li A, Feng F, Jiang Q, Sun H, Chai Y, et al. Effect of the hyaluronic acid-poloxamer hydrogel on skin-wound healing: in vitro and in vivo studies. Animal Model Exp Med 2019;2:107–13. https://doi.org/10.1002/AME2.12067.
[23] Shi C, Zhang Y, Wu G, Zhu Z, Zheng H, Sun X, et al. Hyaluronic acid-based reactive oxygen species-responsive multifunctional injectable hydrogel platform accelerating diabetic wound healing. Adv Healthcare Mater 2023. https://doi.org/10.1002/ADHM.202302626.
[24] Shakya S, Wang Y, MacK JA, Maytin EV. Hyperglycemia-induced changes in hyaluronan contribute to impaired skin wound healing in diabetes: review and perspective. Int J Cell Biol 2015;2015. https://doi.org/10.1155/2015/701738.
[25] Xin Y, Xu P, Wang X, Chen Y, Zhang Z, Zhang Y. Human foreskin-derived dermal stem/progenitor cell-conditioned medium combined with hyaluronic acid promotes extracellular matrix regeneration in diabetic wounds. Stem Cell Res Ther 2021;12. https://doi.org/10.1186/S13287-020-02116-5.
[26] Zhang Y, Zheng Y, Shu F, Zhou R, Bao B, Xiao S, et al. In situ-formed adhesive hyaluronic acid hydrogel with prolonged amnion-derived conditioned medium release for diabetic wound repair. Carbohydr Polym 2022;276. https://doi.org/10.1016/J.CARBPOL.2021.118752.
[27] Palumbo FS, Pitarresi G, Fiorica C, Matricardi P, Albanese A, Giammona G. In situ forming hydrogels of new amino hyaluronic acid/benzoyl-cysteine derivatives as potential scaffolds for cartilage regeneration. Soft Matter 2012;8. https://doi.org/10.1039/c2sm07310b.
[28] Salvatore Palumbo F, Fiorica C, Paola Carreca A, Iannolo G, Pitarresi G, Amico G, et al. Modulating the release of bioactive molecules of human mesenchymal stromal cell secretome: heparinization of hyaluronic acid-based hydrogels. Int J Pharm 2024;653:123904. https://doi.org/10.1016/J.IJPHARM.2024.123904.
[29] Chinnici CM, Amico G, Monti M, Motta S, Casalone R, Li Petri S, et al. Isolation and characterization of multipotent cells from human fetal dermis. Cell Transplant 2014;23:1169–85. https://doi.org/10.3727/096368913X668618.
[30] Chinnici CM, Amico G, Gallo A, Iannolo G, Cuscino N, Vella S, et al. Small extracellular vesicles from human fetal dermal cells and their MicroRNA cargo: KEGG signaling pathways associated with angiogenesis and wound healing. Stem Cell Int 2020;2020. https://doi.org/10.1155/2020/8889379.
[31] Wiśniewski JR, Zougman A, Nagaraj N, Mann M. Universal sample preparation method for proteome analysis. Nat Methods 2009;6:359–62. https://doi.org/10.1038/NMETH.1322.
[32] Meissner F, Scheltema RA, Mollenkopf HJ, Mann M. Direct proteomic quantification of the secretome of activated immune cells. Science 2013;340:475–8. https://doi.org/10.1126/SCIENCE.1232578.
[33] Spanò DP, Bonelli S, Calligaris M, Carreca AP, Carcione C, Zito G, et al. High-resolution secretome analysis of chemical hypoxia treated cells identifies putative biomarkers of chondrosarcoma. Proteomes 2022;10. https://doi.org/10.3390/PROTEOMES10030025.
[34] Rappsilber J, Ishihama Y, Mann M. Stop and go extraction tips for matrix-assisted laser desorption/ionization, nanoelectrospray, and LC/MS sample pretreatment in proteomics. Anal Chem 2003;75:663–70. https://doi.org/10.1021/AC026117I.
[35] Cox J, Mann M. MaxQuant enables high peptide identification rates, individualized p.p.b.-range mass accuracies and proteome-wide protein quantification. Nat Biotechnol 2008;26:1367–72. https://doi.org/10.1038/NBT.1511.
[36] Chen EY, Tan CM, Kou Y, Duan Q, Wang Z, Meirelles GV, et al. Enrichr: interactive and collaborative HTML5 gene list enrichment analysis tool. BMC Bioinf 2013;14. https://doi.org/10.1186/1471-2105-14-128.
[37] Hallmann R, Horn N, Selg M, Wendler O, Pausch F, Sorokin LM. Expression and function of laminins in the embryonic and mature vasculature. Physiol Rev 2005;85:979–1000. https://doi.org/10.1152/PHYSREV.00014.2004.
[38] Chinnici CM, Iannolo G, Cittadini E, Carreca AP, Nascari D, Timoneri F, et al. Molecular sciences extracellular vesicle-derived microRNAs of human wharton's jelly mesenchymal stromal cells may activate endogenous VEGF-A to promote angiogenesis. https://doi.org/10.3390/ijms22042045; 2021.
[39] Gaetani M, Chinnici CM, Carreca AP, Di Pasquale C, Amico G, Conaldi PG. Unbiased and quantitative proteomics reveals highly increased angiogenesis induction by the secretome of mesenchymal stromal cells isolated from fetal rather than adult skin. J Tissue Eng Regen Med 2018;12:e949–61. https://doi.org/10.1002/TERM.2417.
[40] Chinnici CM, Pietrosi G, Iannolo G, Amico G, Cuscino N, Pagano V, et al. Mesenchymal stromal cells isolated from human fetal liver release soluble factors with a potential role in liver tissue repair. Differentiation 2019;105:14–26. https://doi.org/10.1016/J.DIFF.2018.12.001.
[41] Baldassarro VA, Perut F, Cescatti M, Pinto V, Fazio N, Alastra G, et al. Intra-individual variability in the neuroprotective and promyelinating properties of conditioned culture medium obtained from human adipose mesenchymal stromal cells. Stem Cell Res Ther 2023;14. https://doi.org/10.1186/S13287-023-03344-1.
[42] Md Fadilah NI, Mohd Abdul Kader Jailani MS, Badrul Hisham MAI, Sunthar Raj N, Shamsuddin SA, Ng MH, et al. Cell secretomes for wound healing and tissue regeneration: next generation acellular based tissue engineered products. J Tissue Eng 2022;13. https://doi.org/10.1177/20417314221114273.
[43] Palumbo FS, Fiorica C, Pitarresi G, Agnello S, Giammona G. Interpenetrated 3D porous scaffolds of silk fibroin with an amino and octadecyl functionalized hyaluronic acid. RSC Adv 2015;5:61440–8. https://doi.org/10.1039/C5RA09400C.
[44] Baldassarro VA, Giraldi V, Giuliani A, Moretti M, Pagnotta G, Flagelli A, et al. Poly(L-lactic acid) scaffold releasing an α 4 β 1 integrin agonist promotes nonfibrotic skin wound healing in diabetic mice. Cite this. ACS Appl Bio Mater 2023;6:308. https://doi.org/10.1021/acsabm.2c00890.
[45] Park SR, Kim JW, Jun HS, Roh JY, Lee HY, Hong IS. Stem cell secretome and its effect on cellular mechanisms relevant to wound healing. Mol Ther 2018;26:606–17. https://doi.org/10.1016/J.YMTHE.2017.09.023.
[46] FDA Floats Regulating Hyaluronic Acid Products as Drugs, Not Devices | RAPS n.d. https://www.raps.org/News-and-Articles/News-Articles/2018/12/FDA-Floats-Regulating-Hyaluronic-Acid-Products-as (accessed February 2, 2024).
[47] Balasubramanian GV, Chockalingam N, Naemi R. The role of cutaneous microcirculatory responses in tissue injury, inflammation and repair at the foot in diabetes. Front Bioeng Biotechnol 2021;9. https://doi.org/10.3389/FBIOE.2021.732753.
[48] Yousefi S, Qin J, Dziennis S, Wang RK. Assessment of microcirculation dynamics during cutaneous wound healing phases in vivo using optical microangiography. J Biomed Opt 2014;19:076015. https://doi.org/10.1117/1.JBO.19.7.076015.
[49] van Balkom BWM, Gremmels H, Giebel B, Lim SK. Proteomic signature of mesenchymal stromal cell-derived small extracellular vesicles. Proteomics 2019;19:1800163. https://doi.org/10.1002/PMIC.201800163.
[50] Lin Z-Q, Kondo T, Ishida Y, Takayasu T, Mukaida N. Essential involvement of IL-6 in the skin wound-healing process as evidenced by delayed wound healing in IL-6-deficient mice. J Leukoc Biol 2003;73:713–21. https://doi.org/10.1189/JLB.0802397.
[51] Caley MP, Martins VLC, O'Toole EA. Metalloproteinases and wound healing. Adv Wound Care 2015;4:225–34. https://doi.org/10.1089/WOUND.2014.0581.
[52] Huang H, Zhang Q, Liu J, Hao H, Jiang C, Han W. Granulocyte-colony stimulating factor (G-CSF) accelerates wound healing in hemorrhagic shock rats by enhancing angiogenesis and attenuating apoptosis. Med Sci Mon Int Med J Exp Clin Res 2017;23:2644–53. https://doi.org/10.12659/MSM.904988.
[53] Lazaro JL, Izzo V, Meaume S, Davies AH, Lobmann R, Uccioli L. Elevated levels of matrix metalloproteinases and chronic wound healing: an updated review of clinical evidence. J Wound Care 2016;25:277–87. https://doi.org/10.12968/JOWC.2016.25.5.277.
[54] Lee E, Vaughan DE, Parikh SH, Grodzinsky AJ, Libby P, Lark MW, et al. Regulation of matrix metalloproteinases and plasminogen activator inhibitor-1 synthesis by plasminogen in cultured human vascular smooth muscle cells. Circ Res 1996;78:44–9. https://doi.org/10.1161/01.RES.78.1.44.